machines

MDPI

Article

Effect of Combined Film Cooling and Swirl on the Thermal Performance of a Contoured High Pressure Turbine Vane of a Modern Turbofan Engine: A Numerical Study

Djihane Mazouz [1], Zakaria Mansouri [2,*] and Salaheddine Azzouz [1]

[1] Laboratory of Energy Systems Technologies (LTSE), Department of Process Engineering and Energetics, National Higher School of Technology and Engineering, Annaba 23005, Algeria
[2] Department of Engineering, Nottingham Trent University, Clifton Campus, Nottingham NG11 8NS, UK
* Correspondence: zak.mansouri@ntu.ac.uk

Abstract

Modern high-pressure turbine (HPT) nozzle guide vanes (NGVs) operate under non-uniform inlet conditions, including hot streaks and swirl, which can induce complex flow phenomena and uneven thermal loading. These effects, particularly at the hub-vane corner, can compromise NGV durability, yet the combined influence of swirl and film cooling remains underexplored. The objective of this study is to investigate the aerothermal behaviour of contoured first-stage NGVs under varying swirl intensities and directions to improve understanding of hub and corner thermal protection and failure mechanisms. Steady, compressible RANS simulations were conducted with the k-ω SST turbulence model. A vane with a contoured hub and multiple film cooling rows was designed and analysed under axial and swirling inflows, both clockwise and counter-clockwise, with swirl numbers of Sn = ±0.2 and ±0.4. Axial flow achieved the highest area-averaged film cooling effectiveness (FCE) of 0.617. Negative swirl (Sn = −0.4) improved suction-side corner FCE to 0.215 but reduced pressure-side cooling, whereas positive swirl (Sn = 0.4) improved pressure-side cooling but reduced suction-side FCE to 0.043. Corner temperatures under positive swirl reached 1780 K, consistent with promoting failure, while negative swirl reduced corner temperatures to 1516 K. Aerodynamic losses increased with swirl, with negative swirl generating 5.78% higher total pressure losses than the axial baseline. Swirl altered the corner vortex topology, affecting boundary layer interactions and local heat transfer. These results highlight a trade-off between thermal protection and aerodynamic efficiency, emphasising that optimising NGV performance requires careful design of hub cooling and consideration of swirl direction and intensity.

Keywords: heat transfer; film cooling; nozzle guide vane; thermal loading; numerical simulation

Academic Editor: Ahmed Abu-Siada

Received: 2 February 2026
Revised: 8 March 2026
Accepted: 16 March 2026
Published: 18 March 2026

1. Introduction

A real-world turbine engine operates under non-uniform inlet conditions such as hot-streak and swirling from the combustion chamber. This swirl serves to mix the air and fuel to stabilise the flame, to prevent it from extinguishing, and to minimise pollutants by reducing the formation of nitrogen oxides (NOx) [1], and ensure highly efficient combustion. However, it introduces flow complexities in the stage adjacent to the combustor, affecting essential parameters such as the thermal loading distribution on the nozzle guide vanes (NGVs), total pressure, and secondary flow characteristics [2]. Consequently, understanding the behaviour of gas turbines under swirling flow conditions is vital for optimising the

turbine's overall performance. For example, Figure 1 presents a high-pressure turbine (HPT) segment of a turbofan engine comprising two nominally identical nozzle guide vanes. The segment incorporates both internal and film cooling. It is evident that the NGV on the right is in satisfactory condition, whereas the NGV on the left exhibits marked deterioration. The latter displays several small cracks at the vane–hub intersection (corner), incurred after extended service under elevated thermal loading. It may be reasonably inferred that the left-hand NGV is positioned directly downstream of the combustor's flame nozzle (fuel injectors). Consequently, the observed corner cracking can be attributed to thermal-stress fatigue induced by the hot streak.

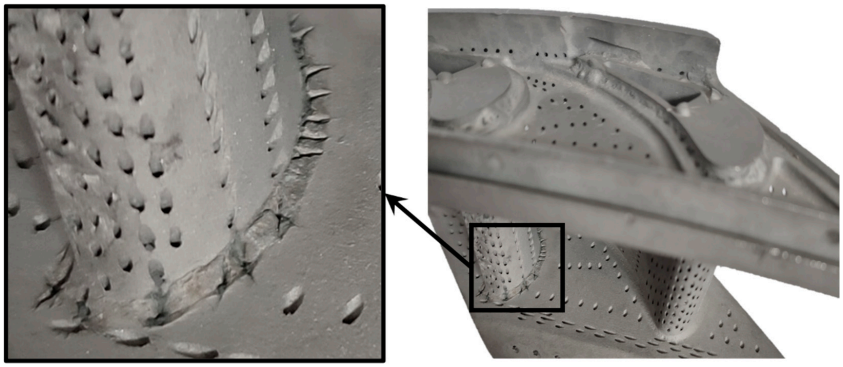

Figure 1. Two nozzle guide vanes of a high-pressure turbine showing the left NGV featuring small cracks at the vane–hub corner.

For this, numerous papers have examined this phenomenon, particularly in the absence of film cooling. Zhang et al. [3] carried out an unsteady numerical study on a GE-E3 HP turbine, investigating the behaviour of the high-pressure turbine (HPT) with the swirl effect. The results revealed a clear link between the swirl in the flow pattern at the blade surface. In addition, the swirl modifies the heat transfer coefficient (HTC) distribution on the blade surface. Qureshi et al. [4] carried out a comprehensive numerical and experimental research into the aerodynamic and heat transfer impact of a high swirl on high-pressure turbine vanes. The results showed that the stagnation point shifts toward the pressure side (PS) at the hub and toward the suction side (SS) at the casing. Due to changes in the flow profiles at the end-wall and vane surfaces, a redistribution of boundary-layer fluid occurred, accumulating in specific regions and dispersing in others. Nusselt numbers exhibit significant variations with increasing swirl intensity. This is due to the accumulation and dissipation of boundary layer (BL) fluid associated with the divergence and convergence of surface streamlines, as well as variations in the vane loading and hence surface velocity. In another work, Qureshi et al. [5] conducted a thorough computational and experimental investigation to examine the effect of a high inlet swirl on the heat transfer characteristics of a high-pressure (HP) rotor and casing. The results show that measurements of heat transfer at three locations on the rotor surface demonstrate that the swirl effect on the rotor is reduced compared to the nozzle guide vane (NGV), even though an increase in the Nusselt number on the surface of the rotor has been found to occur with the inlet swirl. Beard et al. [6] conducted an experimental and computational analysis of inlet swirl and its effect on transonic efficiency in a turbine stage. They conducted the experiments using the unshrouded MT1 high-pressure turbine, installed at the Oxford Turbine Research Facility (OTRF). Computational fluid dynamics (CFD) of the complete stage was conducted using the Hydra solver from Rolls-Royce. They performed both steady-state and unsteady-state solutions for both the base case of a uniform inlet and for a case with an inlet swirl. The main reason for the reduction in turbine efficiency due to inlet swirl is the generation of additional losses in the vane passage. From the static pressure data taken on the surface of

the vane, it was determined that the inlet swirl strongly influenced the load distribution on the vane. The most noticeable impact was on the front part of the vane surface. Schmid and Schiffer [7] numerically studied the impact of inlet swirl on the behaviour of turbine vane cascade, considering swirl intensity, clocking position, and swirl orientation. Regarding the swirl number effect, the results indicated that a vortex core develops and expands more rapidly, impinging on the end-wall further upstream as the swirl number increases. Speaking about the swirl's position and orientation influences, a significant influence is produced on the flow behaviour and performance in the turbine blade passage. A recent work by Jacobi et al. [8] experimentally investigated steady and unsteady impacts of combustor swirl on first-vane aerodynamics in a high-speed linear cascade NGV, supplemented by extensive eddy simulations. The study indicates significant flow instability affecting heat transfer, characterised by a continuous vortical structure oscillating at the leading edge due to swirl–vane interactions, together with transitory horseshoe vortex behaviour resulting from incidence variations.

To gain deeper insights into the complex interplay between film cooling and swirling flow, several researchers have investigated the combined effects of swirling flow and film cooling schemes replicating real-world engine-like conditions. As demonstrated by Ito et al. [9] study, film cooling is an efficient technique whereby a layer of cooling air flows over the turbine surface, achieving remarkable heat flux reduction through careful coolant injection and mainstream flow interaction. However, under swirling inflow conditions, the cooling effectiveness becomes highly sensitive to unsteady combustor flow interactions. For instance, Hou et al. [10] computationally investigated the effect of inlet swirl on leading edge film cooling performance. They found that while swirl enhances coolant-mainstream mixing and creates a downstream-damaging vortex, trenched holes present higher cooling performance under various swirl intensities and blowing ratios. Although trenched holes cannot eliminate the swirling mainstream flow patterns, they ensure superior lateral coolant dispersion and prevent its rotation downstream. Consequently, they outperform round holes, which peak at a 2.0 blowing ratio but yield lower efficiency. Bacci et al. [11] conducted experimental measurements to establish the efficiency of the adiabatic film in the central sector vanes and to evaluate the performance of cooling the film in swirling flow conditions. According to the results, the swirling main flow has a significant impact on the film's cooling behaviour. The position of the leading-edge stagnation points and the properties of the pressure- and suction-side film coverings have been observed to differ between the central airfoil and its neighbouring airfoils. In addition, as the clock is positioned between the swirl and the vane, the distribution of film efficiency is significantly affected. In line with this, Du et al. [12] reported on the effects of inlet swirl flow on film cooling efficiency using a pressure-sensitive paint (PSP) experimental approach and a numerical method. Given mass flow ratios (MFRs) ranging from 0.5 to 2%, the film-cooling efficiency with the purge slot was significantly enhanced. At high MFRs, the coverage of the film at the slot exits is significantly enhanced. A positive swirl with a lower negative swirl can improve the cooling efficiency of the film inside the channel. Xu et al. [13] used PSP and numerical simulations to examine film-cooling characteristics under swirl conditions. They found that film migration is not directly proportional to swirl intensity. At low swirl ($S_n = 0.3$), migration is insignificant, reducing area-averaged η by up to 3.0%. At high swirl ($S_n = 0.45$), migration becomes pronounced, causing an 11.9% maximum reduction in η. Increasing the coolant flow reduces migration to a limited extent. For full film-cooling vanes, film migration is partially caused by swirling vortices but predominantly results from leading-edge film migration, as swirling inflow shifts the stagnation line and modifies cooling airflow. Lu et al. [14] has determined the improvement in effusion cooling efficiency of fan-shaped holes in comparison with cylindrical holes under swirl

flows from 1.2 to 6.0 blowing ratios (BRs) in a swirl-stabilised combustor based on the thermochromic liquid crystal (TLC) experimental method, whilst conducting k − ω SST Reynolds-Averaged Navier–Stokes (RANS) calculations to assess the interaction between film coverage and swirl flows so as to highlight how the cooling effects differ in the physical mechanism. The findings showed that cooling air tends to be dissipated more readily at low BR due to the swirl effect, whereas higher BR increases cooling air resistance against swirl flow. Furthermore, they demonstrated that fan-shaped holes provided a 19.7–53.2% higher cooling effectiveness in the impact zones and a more significant 39.1–84.2% improvement in the corner recirculation zone. A three-dimensional RANS simulation of an HPT vane equipped with several rows of fan-shaped holes on the pressure and suction sides, as well as a leading-edge (LE) showerhead, was performed by Insinna et al. [15]. Inlet swirl is detrimental from a vane coverage perspective, particularly from a showerhead perspective. As a result of swirl core convection inside the passages and their interaction with the secondary flows, considerable changes occur in coolant coverage with respect to the uniform inlet case. Giller and Schiffer [16] carried out an experimental study to reveal the impact of swirling combustion chamber flow on turbine nozzle guide vanes in the cascade test rig at Technische Universität Darmstadt, varying the swirl intensities and blowing ratio. Their study concluded that taking into account the swirling inflow produces major shifts in the flow field with higher losses compared to an axial inflow. It also affects the formation and the adiabatic effectiveness of the cooling film. Observations indicate the dominance of the swirl in the secondary flow field, which remains visible beyond the vane passages. Nevertheless, the swirling and turbulent inflow counteracts the cooling air lift-off effect. Li et al. [17] used RANS simulations to analyse the effect of counter-clockwise swirling inflow on a film-cooled vane. For swirl numbers (0.6, 0.8, and 1.0), the swirl alters the main flow, moves the horseshoe vortex downstream, creates a recirculation vortex, and increases the heat transfer coefficient. This expands the high heat transfer regions on the vane end-wall. As swirl intensity increases, film cooling effectiveness rises by 27% at the first row and 9% at the third row compared to non-swirling conditions. Werschnik et al. [18–20] carried out several experimental studies to investigate how swirling flow affects turbine film cooling performance, taking into account different MFR and clocking positions. Their findings indicate that swirl flow increases overall end-wall heat transfer coefficients in terms of Nusselt number compared to axial flow, while simultaneously reducing film cooling efficiency, particularly at lower MFR. Furthermore, swirl flow orientation potentially impacts turbine performance. The influence of swirl flow on the efficiency of end-wall film cooling was evaluated by Zhang et al. [21] through experiments. Five configurations of end-wall film cooling were evaluated, each with a different clocking position for the swirling flow. There is an opposite trend in the cooling efficiency of the film in the upstream and downstream regions under a constant BR. This, according to vortex mixing theory, is the result of the interaction between the passage secondary flow and the swirling flow. Downstream, there was a substantial interaction of mainstream and swirling flow closer to the trailing edge (TE). The film cooling of the end-wall is negatively affected by the mainstream flow and the integrated rotating flow.

To the authors' knowledge, the thermal loading of NGV hub corners under the combined influence of film cooling and inflow swirl has not been previously examined. While earlier work by the authors' group investigated swirl effects for flat end-wall configurations [22–25], the present study extends that effort to a more realistic contoured NGV hub platform representative of modern turbofan engine turbines, such as those employed in the CFM LEAP family, where secondary-flow structures and corner heat transfer are significantly influenced by end-wall contouring. The work further introduces a hub-only multi-row film cooling arrangement representative of contemporary first-stage NGV

designs. A systematic parametric investigation is conducted by varying both the direction (clockwise and counter-clockwise) and intensity of the inlet swirl. By comparing swirling and non-swirling inflow conditions, the study provides new insight into the interaction between swirl-induced secondary flows, corner vortices, and film-cooling performance, enabling a vortex-based interpretation of vane–hub corner thermal loading and potential durability risks. Section 2 outlines the numerical methodology and its validation; Section 3 presents the principal findings; and Section 4 summarises the conclusions.

2. Cascade Geometry and Numerical Method

2.1. Cascade Geometry

This study relies on a turbine's first-stage annular cascade NGV developed by the NASA Lewis Research Centre [26,27] as shown in Figure 2a. The cascade is designed with flat end-walls (hub and shroud) for steady axial flow conditions and operates with a pressure ratio (static to total) of 0.6885 between the outlet and the inlet. The geometry of NGV is defined by an axial chord length of 38.23 mm, a solidity of 0.93, and an outflow angle of 67 degrees. The tip radius is 0.254 m. This flat hub cascade has been the subject of multiple numerical investigations under hot-streak and swirl conditions [22–25]. A more realistic contoured NGV hub platform, representative of modern turbofan engine turbines, such as those employed in the CFM LEAP family, is required to be investigated to advance the fundamental understanding of secondary-flow structures and corner heat transfer, which are significantly influenced by end-wall contouring. An updated geometry of this cascade was developed by the authors to replicate modern HPT stages by introducing a contoured platform (hub) in the streamwise direction. As a result, the passage height and the local hub-to-tip ratio vary from inlet to outlet whereas the shroud radius remains constant. Figure 2b shows this contoured cascade with boundary conditions used in the validation section with experimental data. The swirling flow imposed at the cascade inlet is uniform tangential velocity generated by the CFD solver shown in Figure 2c,d.

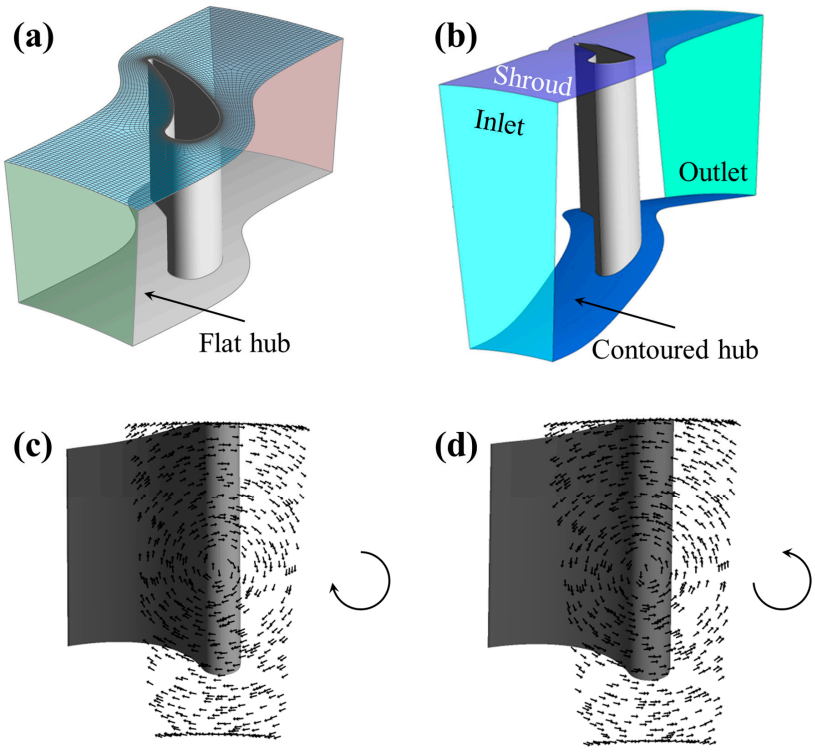

Figure 2. Three-dimensional uncooled NGV geometries with (**a**) flat hub cascade, (**b**) contoured hub cascade, (**c**) positive swirl condition, and (**d**) negative swirl condition.

For this study, a further design update included a cooling arrangement located at the hub, which comprises four distinct cooling schemes, as illustrated in Figure 3. A slot representing the change from combustor platform to turbine platform followed by a first cooling row consisting of 14 holes is strategically located upstream of the vane LE. These are complemented by two additional cooling rows near the vane pressure side where the second contains five holes and the third contains three holes. Each of these holes is inclined at an angle of 25° with respect to the contoured platform surface. This setup focuses on cooling the PS region only due to computational limitations although modern NGV platforms such as the one in Figure 1 are aggressively cooled at both PS and SS. Each present cooling scheme employs separate air supplies, channelling the air through a plenum chamber prior to its injection onto the vane surface.

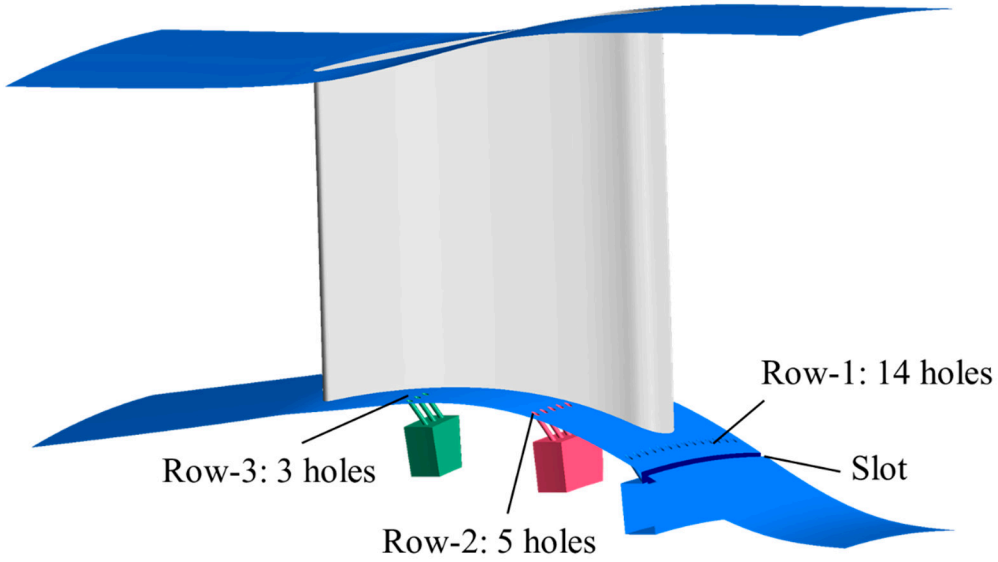

Figure 3. Film cooling arrangement at the NGV hub.

2.2. Numerical Methodology

Ansys CFX 19.R3 software was used to conduct numerical simulations. It employs a finite volume method for discretising the governing equations. Reynolds-Averaged Navier–Stokes (RANS) equations were used to model the flow, which is considered as steady and compressible. This assumption is consistent with the original NASA annular cascade configuration, which was designed and experimentally investigated under steady axial inflow conditions. Although the introduction of swirl may generate local unsteadiness and vortex-dominated structures, the imposed swirl in the present study does not correspond to a periodic transient forcing. Instead, the flow can be reasonably characterised through its time-averaged behaviour, for which steady RANS provides an efficient modelling approach. Steady RANS has been widely employed to characterise complex swirling flows and their time-averaged aerothermal characteristics in lean-burn combustors [28–30], further supporting its suitability for the present study. To capture temperature variations, the total energy equation was solved, considering the transport of enthalpy, effects of kinetic energy and viscous dissipation. A second-order upwind accurate numerical discretisation scheme was employed. The turbulence model adopted is the two-equation $k - \omega$SST with Gamma-Theta-model for boundary layer transition prediction [31,32]. Convergence was achieved when all governing equations' root mean square (RMS) residuals reached a tolerance of 1×10^{-5}.

2.3. Mesh and Boundary Conditions

To validate the present numerical method with experimental data from [26,27], two cascade configurations are considered including the original flat cascade and the new contoured cascade. The mesh type is hybrid and was generated using Fluent Meshing. A grid independence study was conducted to ensure numerical accuracy. For the original flat cascade, three different meshes were built including a coarse mesh with 0.59 million nodes, a medium mesh with 1.234 million nodes, and a fine mesh with 2.7 million nodes. For the contoured uncooled cascade (Figure 2b), three meshes were created with the following resolutions: coarse mesh of 2 million elements, medium mesh of 5 million elements, and fine mesh of 7 million elements. For the cooled NGV a mesh of 10 million elements was created. Based on comparisons with established mesh densities from similar hub-cooling problems in the very recent literature, as shown in Table 1, the current mesh was determined to be computationally efficient and accurate for capturing the key flow features. To precisely capture boundary-layer development, a refined mesh was generated in the vicinity of all the cascade walls. The dimensionless height of the first cell "y+" value was kept below 0.8 through the entire cascade domain, including within the cooling holes and at the hub–vane corner. This ensures that the viscous sublayer is resolved to predict any boundary layer transition and to achieve improved accuracy in near-wall quantities. Since turbulence is treated using the k − ωSST model with Gamma-Theta formulation following Menter et al. [31], the grid must have a y+ of ≈1 to capture the laminar and transitional boundary layers correctly. If y+ is too large (i.e., >5), the transition onset location shifts upstream as y+ increases. A wall normal grid expansion ratio of 1.1 was also used as recommended in [31]. The results of the mesh independence study are presented in the subsequent section.

Table 1. Comparison of the present mesh resolution with those from the recent literature.

	Present Study ($\times 10^6$)	**Literature ($\times 10^6$)**				
Size	10	8.6 [33]	8 [34]	8 [35]	6.6 [36]	4.03 [37]

For the validation cases using both the uncooled flat and contoured cascades (Figure 2), the inlet boundary was positioned one axial chord upstream of the LE, while the outlet boundary was located one axial chord downstream of the TE. A pair of periodic boundary conditions was applied in the pitchwise direction simulations, as shown in Figure 2. The specific boundary conditions imposed on the domain are as follows: a total pressure condition with high turbulence intensity of 10% and a total temperature of 1780 K was set at the mainstream inlet. An average static pressure of 69,760.5 Pa is established at the domain's outlet. Non-slip, smooth and adiabatic boundary conditions are assumed for all walls.

For the cooled cascade (Figure 3), the inlet boundary was also positioned at one axial chord upstream of the LE. To represent the swirl effect, a tangential velocity component was applied at this boundary. Equation (1) defines the swirl number S_n, which was used to quantify the swirling flow's intensity, where U and W are the averaged axial velocity and the averaged tangential velocity, respectively. It should be noted that the swirl number is here defined as a simplified term representing the ratio between the velocities, as indicated in the references [22,23]. Both clockwise and counter-clockwise swirl orientations were examined, along with a range of swirl numbers. The effect of swirling flow on the cooled NGV's aerothermal performance can be evaluated by altering the swirl's intensity and direction. Table 2 summarises the considered swirl intensities and directions at the inlet.

$$S_n = W/U \quad (1)$$

Table 2. Investigated swirl intensities and directions.

Case	Baseline (Axial)	Clockwise		Counter-Clockwise	
Swirl number	$S_n = 0$	$S_n = 0.2$	$S_n = 0.4$	$S_n = -0.2$	$S_n = -0.4$

At the inlets of the three cooling plenums a turbulence intensity of 5% was imposed with a total temperature of 883.15 K. A mass flow ratio (MFR), which is the mass of cooling air to the mainstream hot gas flow, was considered constant at 1. Werschnik et al. [20] who experimentally investigated MFR = 0.4, 0.9, 2.0, and 2.9 at various axial and swirling flow conditions and stated that cooling of the entire end-wall surface requires an MFR of slightly greater than the studied value of 0.9. MFR is defined in Equation (2).

$$MFR = \frac{\rho_c \, u_c}{\rho_\infty \, u_\infty} \tag{2}$$

where ρ_c and u_c are coolant density and velocity, and ρ_∞ and u_∞ are the hot mainstream density and velocity, respectively.

2.4. Numerical Validation

Two validations were conducted. The first used the flat-hub cascade (Figure 2a) to evaluate the accuracy of the numerical method, as presented in Figure 4a. The second validation used the new contoured hub cascade (Figure 2b) to assess the effect of end-wall contouring on the flow behaviour, as shown in Figure 4b. The pressure ratio results on the vane mid-span are compared with the available experimental data [26,27]. Figure 4a shows no remarkable difference between the results of the different meshes as they all align very well with the experimental data. Figure 4b indicates that the contoured shape of the hub has no effect on the PS pressure ratio where a favourable pressure gradient develops. In contrast, the contouring alters the pressure ratio at the vane SS leading to higher pressure ratio values before 0.7 of the streamwise direction indicating a decelerated flow with lower velocity compared with the experimental case. All meshes exhibit the same profile. Furthermore, Table 3 summarises the area-averaged values of the pressure ratio and the Nusselt number on the vane surface for the three different meshes of the contoured vane. Using the fine mesh as a reference, the coarse mesh exhibited deviations of approximately 1.75% in pressure ratio and 2.54% in Nusselt number, whereas the medium mesh showed significantly smaller discrepancies of 0.63% and 1.12%, respectively. These results indicate that the medium mesh provides a satisfactory compromise between computational cost and accuracy, but the fine 7 million mesh was considered in the cascade passage of the cooled configuration for improved accuracy. Although experimental heat transfer or film-cooling data for the present NGV geometry are not available in [26,27], the numerical method employed has been rigorously validated in the authors' previous studies against measured heat transfer coefficients [24] and wall heat fluxes [38] on rotor blades. The reader is encouraged to consult [24,38] for the validation of the near-wall thermal behaviour.

Table 3. Mesh independence study of the contoured cascade.

Quantity/Size	Coarse	Medium	Fine
Pressure ratio	0.812	0.793	0.798
Nusselt number	1427.51	1376.64	1392.21

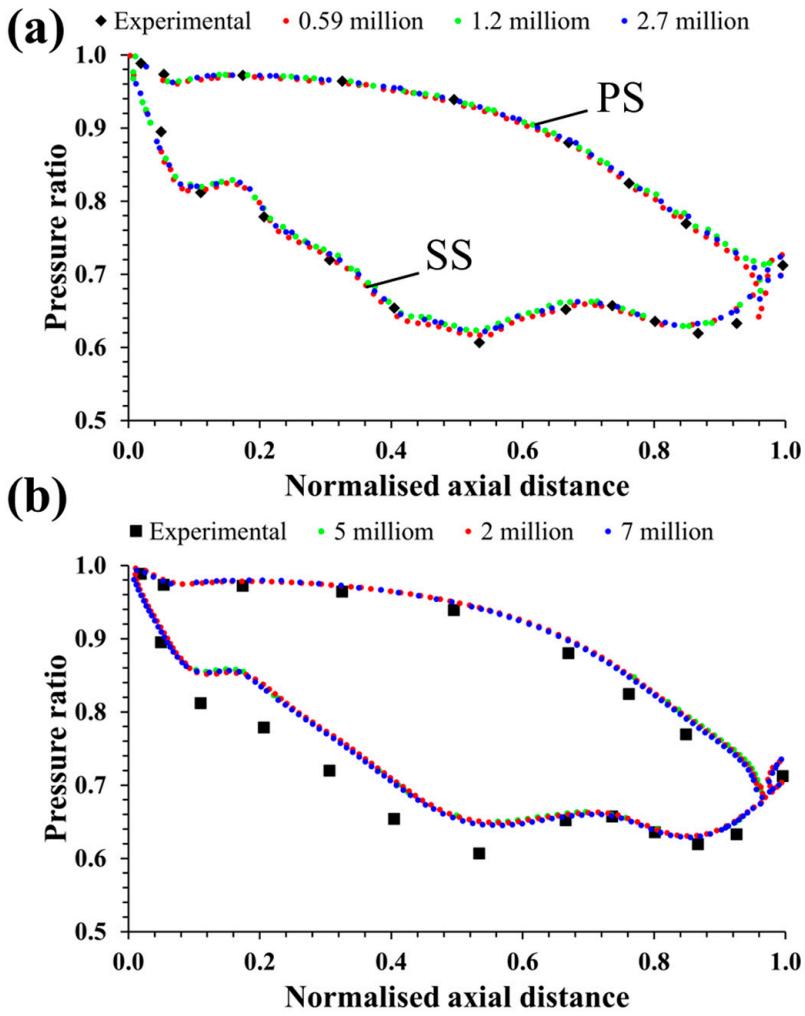

Figure 4. Comparison between computed and measured pressure ratio at the midspan of the vane using (**a**) the original flat cascade and (**b**) the new contoured cascade.

3. Results and Discussion

3.1. Effect of the Swirl on the Film Cooling Effectiveness

The film cooling effectiveness (FCE) is computed based on the local surface temperature T, the hot mainstream T_∞ and coolant T_c temperatures as indicated in Equation (3).

$$\eta = \frac{T_\infty - T}{T_\infty - T_c} \tag{3}$$

The effect of the swirl on the film cooling effectiveness on the hub is shown in Figure 5. For all cases, the FCE is the highest around the LE of the NGV due to the successive rows of cooling sources (e.g., the slot and row-1 of cooling holes). Around the TE region and downstream, the FCE is the poorest indicating that the cool film is lifted from the platform surface as it is being mixed with the wake. This lift-off behaviour is due to the corner vortex formed at the junction of the blade and the hub at the end of the SS as it will be revealed and discussed in Section 3.4. Without swirl (Sn = 0), the PS exhibits a poor FCE compared with the SS that performs very well. This is attributed to the flow deceleration with the increased pressure due to the blade curvature. This effect leads to extending the horseshoe vortex [22] towards the PS and improves mixing with the hot free stream; hence, FCE is affected negatively. When the negative swirl is introduced (Sn = −0.2 and −0.4), the FCE around the PS becomes worse given the flow rotation in the counter-clockwise direction.

This means the flow will have a negative incidence angle leading to a poorer contact with the PS and a better contact with the SS. This is evidenced by flow streamlines in Section 3.2. The negative incidence angle promotes the cooling film at the BL level to shift toward the SS, improving its effectiveness. When the positive swirl is introduced (Sn = 0.2 and 0.4), the FCE around the PS becomes better, but at the SS it becomes poor. Werschnik et al. [19] reported that only the PS corner region receives cooling, whereas very low FCE values are found in the regions between the cooling holes. This observation agrees with the present positive swirl findings in terms of PS cooling, but in the present study the gap between the cooling holes exhibits a high FCE. The difference could be attributed to variations in the NGV geometry and the MFR, which is one in the present work and three in Werschnik et al. [19]. Furthermore, the flow rotation in the clockwise direction induces a positive incidence angle which improves the contact between the cooling flow and the PS whereas it leads to shifting the flow from the SS; consequently, the FCE is reduced at the SS. Overall, the negative swirl is good at improving the FCE of the SS and the positive swirl is good at improving the FCE of the PS. Hence, a trade-off is present, and other criteria must be taken into account such as the NGV aerodynamic loss to weigh the benefit of each swirl direction as it will be revealed in Section 3.6.

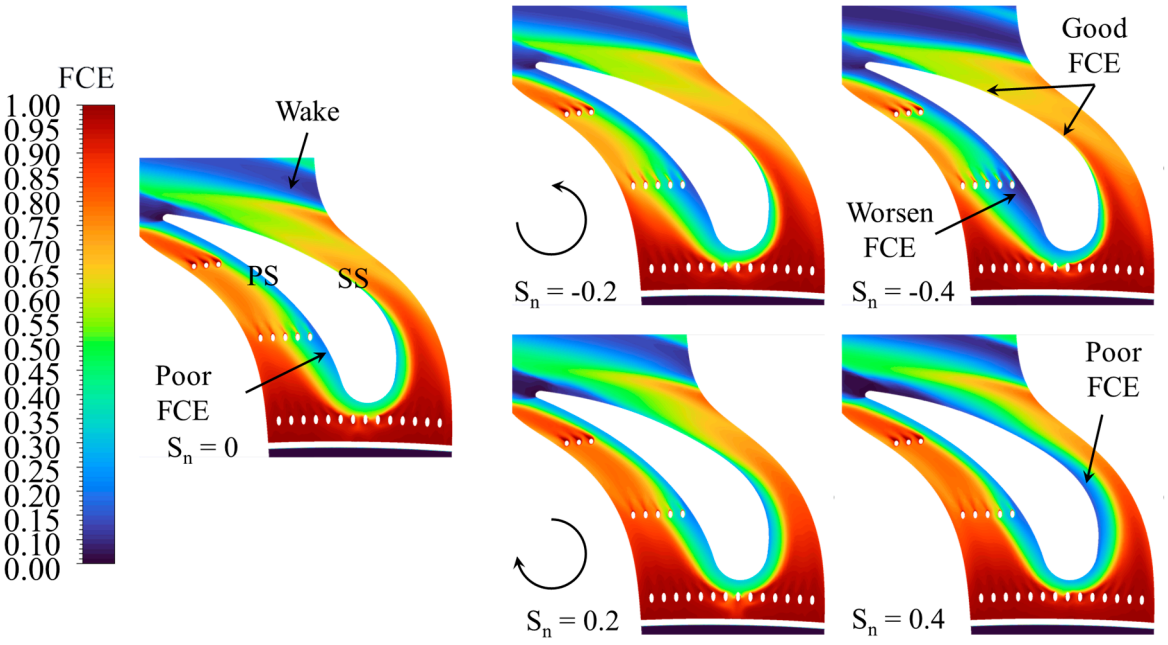

Figure 5. Film cooling effectiveness on the hub surface for all the cases.

The area-averaged FCE at the platform is calculated and plotted in Figure 6 for the different flow cases. Overall, the axial flow condition shows the best FCE, whereas the negative swirl shows the worst FCE. According to Werschnik et al. [19], the turbulence level is expected to increase under swirl conditions, which enhances the mixing of the coolant with the mainstream flow. This supports the higher value of FCE found under the axial flow condition. Moreover, increasing the swirl intensity from Sn = −0.2 to −0.4 has led to a decrease in the FCE from 0.598 to 0.565, respectively. This represents a decrease by 3.7% and 8.59% with respect to the axial flow FCE of 0.617. The positive swirl performs better than the negative swirl with a 0.48% and 4.53% FCE decrease with respect to axial case for Sn = 0.2 to 0.4 respectively. Although these data show that the positive swirl case of Sn = 0.2 is the best case in terms of the highest FCE under swirl condition, it does not reflect local performance such as the presence of hot spots with poor FCE.

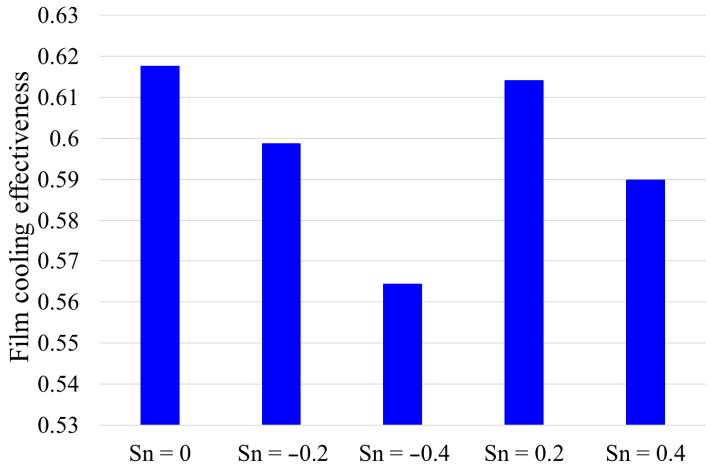

Figure 6. Calculated area-averaged film-cooling effectiveness from the hub surface for all the cases.

3.2. Effect of the Swirl on the 3D Cooling Film Flow

Figure 7 shows the three-dimensional streamlines of the cooling film coming out of the slot and cooling holes. The flow interaction between the cooling rows features a super-imposition behaviour where the cooling film from the precedent row flows above the cooling film from the preceding row. This has led to a continuous improvement of the FCE from the LE to the TE way from the vane corner as illustrated previously in Figure 5. The cool film, as it travels streamwise, mixes with the wake and merges to become relatively hot. At Sn = 0, the cooling flow enters axially with an incidence angle of 0 as shown with the red arrow at the LE. At negative swirl (Sn = −0.2 and −0.4), a negative incidence angle is formed, which leads to shifting the cooling film off of the PS. This is what worsens the FCE at the PS shown previously in Figure 5. However, this negative incidence angle is shown to have a beneficial effect on the FCE at the vane SS by pushing the cooling film towards it. The positive swirl (Sn = 0.2 and 0.4) reverses this behaviour as it induces a positive incidence angle which pushes the cooling film towards the PS and shifts it away from the SS. Consequently, better FCE at the PS and poor FCE at the SS were found (Figure 5). Moreover, the cooling film in the downstream region near the TE is found to be hot indicating that it is lifted off. This indicates that the positive swirl has an adverse effect on the FCE at the SS corner of the vane. The mechanisms leading to this observation will be analysed using surface streamlines in Section 3.4.

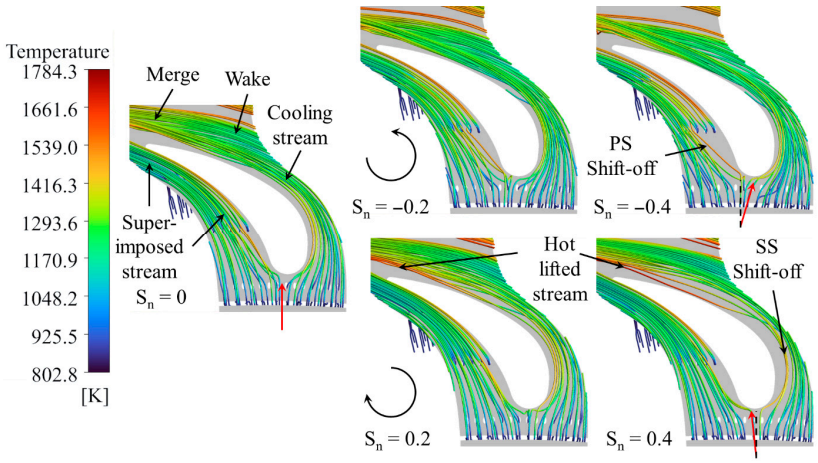

Figure 7. 3D streamlines showing the flow behaviour on the hub surface for all the cases. The red arrow shows the incidence angle.

3.3. Effect of the Swirl on the Corner Thermal Loading

In the Introduction section, it was shown that the vane confronting the hot swirl can undergo high thermal loading leading to the development of small crack at the vane–hub corner (Figure 1). In this section, a cross section of the vane at 5% height away from the platform is used to represent the vane–hub corner, with the FCE plotted on to investigate the thermal load at this region as shown in Figure 8. For both axial and swirl cases, the PS exhibits the worst cooling, despite the presence of cooling rows around this region. The favourable pressure gradient at this region energises the vane–PS boundary layer compared with the weaker BL of the hub, which is under adverse pressure gradient due to the hub's contoured (curved) shape. Thus, the hot BL flow becomes dominant at the PS corner region. When the negative swirl is introduced (Sn = −0.2 and −0.4), the FCE at the PS is improved. The higher the negative swirl, the better the SS corner FCE. As shown in Figure 7 at this swirl condition, the negative incidence angle promotes the flow toward the SS. This contributes to increasing the SS BL acceleration and weakening it; hence, the cool hub BL dominates the corner. When the positive swirl is introduced (Sn = 0.2 and 0.4), the FCE around the SS becomes worse due to the cooling film shifting away (Figure 7). Thus, the SS BL dominates the corner and makes it hotter. Comparing this positive swirl case with Figure 1 showing the SS corner cracks suggests that the positive swirl could be one of the reasons contributing to the vane failure at this region.

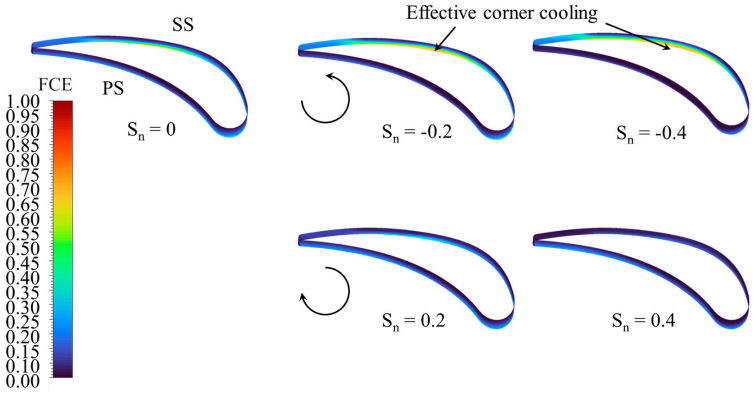

Figure 8. Film-cooling effectiveness on the vane surface near the vane–hub corner for all the cases.

A quantitative analysis of the FCE at the NGV corner can be done using the area-averaged FCE from the 5% vane surface cross section of Figure 8. The results are plotted in Figure 9 and clearly indicate that the negative swirl performs better than both the axial flow and positive swirl in terms of achieving higher SS corner FCE. The FCE reaches 0.203 and 0.215 for Sn = −0.2 and −0.4, respectively, which represents 2.4 and 5 times that of positive swirl cases Sn = 0.2 and 0.4, respectively. This analysis suggests that the negative swirl is the best to prevent high SS corner thermal loading.

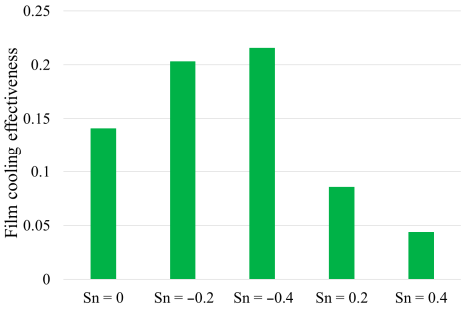

Figure 9. Calculated area-averaged FCE from the vane corner surface for all the cases.

3.4. Effect of the Swirl on the SS Corner Surface Flow

To better understand the mechanism that has led to the improvement of the FCE at the SS corner under negative swirl, surface streamlines are plotted at the SS corner region on both the hub and vane and shown in Figure 10. The surface streamlines are coloured by temperature. For all cases, a corner vortex (CV) is formed at the corner near the TE of the vane. Mechanisms leading to the formation of this vortex are well-established in the literature [22,24]. This is due to the interaction of the vane BL and hub BL under adverse pressure gradient in this region, causing the BLs to be wrapped around each other forming a vortex. At negative swirl (Sn = −0.2 and −0.4), the CV features cool temperatures reaching as low as 1516 K compared to the surface flow coming from the LE region which is at 1780 K. This indicates that the dominant BL forming the vortex is that from the hub. It has already been revealed that the negative swirl pushes the cooling film towards the vane SS contributing to weakening it through acceleration (higher adverse pressure gradient). The hub BL becomes stronger and tends to shift towards the low-pressure region transporting a portion of the cooling film to the SS corner. Under positive swirl (Sn = −0.2 and −0.4), the CV is the hottest among the other cases reaching 1780 K. This indicates that the dominant BL forming the CV is the hot SS BL as it is being energised by the clockwise rotation momentum of the swirl. Moreover, the introduction of swirl motion to the vane flow has not suppressed the CV nor changed its location but rather it altered its topology.

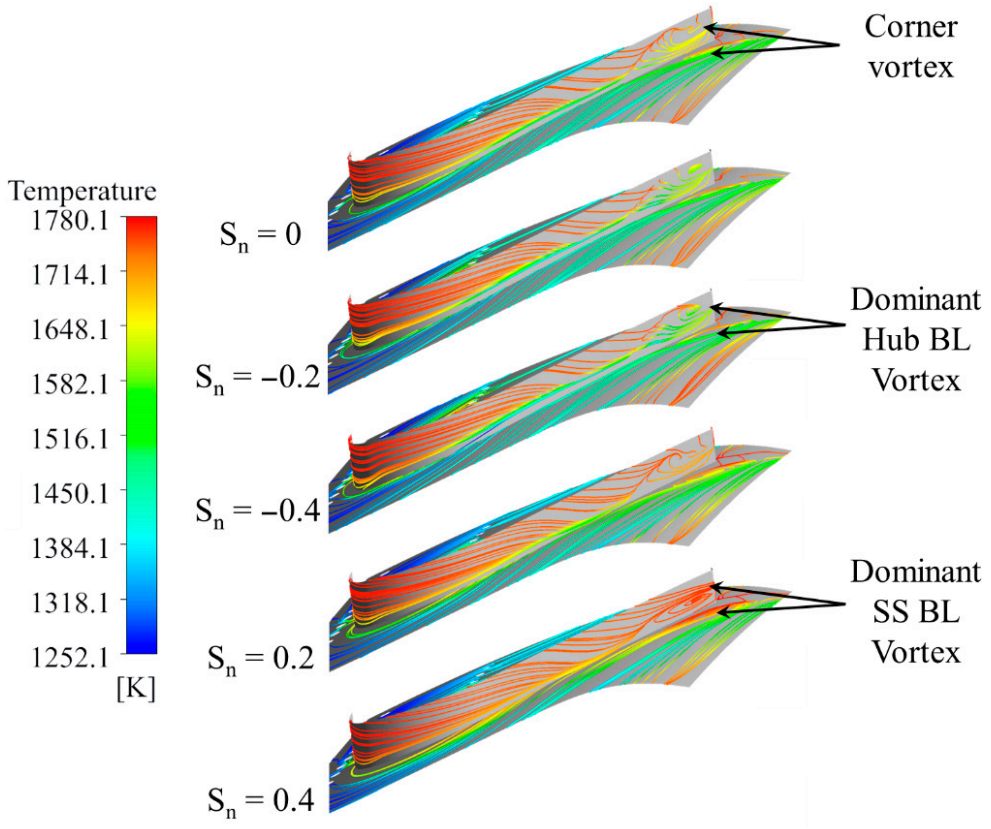

Figure 10. Surface streamlines at the SS corner coloured with temperature for all the cases.

3.5. Effect of the Swirl on the Hub Heat Transfer

The wall boundary condition was set to adiabatic in order to compute the wall temperature presented in the previous sections; however, this prevents the CFD solver from directly obtaining the wall heat flux. In addition, the present simulations do not account for conjugate heat transfer. Therefore, the heat transfer coefficient was estimated using near-wall flow properties, as described in [24,25], and subsequently employed to compute

the Nusselt number. The heat transfer coefficient will be interpreted primarily as indicative of trends and mechanisms rather than as a precise quantitative prediction. Nusselt number (Nu) was used to describe the heat transfer behaviour at the vane–hub. It is defined as follows:

$$Nu = \frac{HTC \times C_{ax}}{\lambda} \tag{4}$$

where HTC is the heat transfer coefficient, C_{ax} is the vane axial chord, and λ is the thermal conductivity of the hot fluid. The HTC can be computed from the following:

$$HTC = \frac{Q}{(T_{\text{flow}} - T_{\text{wall}})} \tag{5}$$

where Q is the heat flux, T_{flow} is the near-wall flow temperature, and T_{wall} is the cooled hub temperature. The heat fluxed is estimated as $Q = \rho c_p v^*$ with ρ is the near wall air density, c_p is the near wall air heat capacity, and v^* is a characteristic velocity inside the boundary layer's logarithmic region. This characteristic velocity depends on the turbulent kinetic energy and wall shear stress as detailed in [24,25].

The surface heat transfer under both axial and swirl conditions is of importance to this work. The Nusselt number distribution of the hub surface was calculated and plotted in Figure 11 for all the cases. Overall, four major regions exhibit a remarkable alteration of Nu distribution: the LE due to the horseshoe (HS vortex, downstream the cooling holes due to the super-imposed stream (SIS) effects, the wake zone due to the flow mixing, and the CV region due to the vortex presence). These regions feature high heat transfer, with the wake region exhibiting the highest Nu. Generally, high heat transfer is linked to high turbulent kinetic energy (TKE) according to Equation (4). The turbulent phenomena mentioned (HS vortex, SIS, wake, and CV) all feature an increased TKE compared to the free stream due to the higher flow shear stress. Introducing the swirl motion does not have a significant effect in altering the Nu distribution, except at the wake zone at the SS near the TE. The positive swirl is seen to improve the heat transfer at the SS near the TE which confirms why the SS corner was found to be hotter compared with the negative swirl case at the same region.

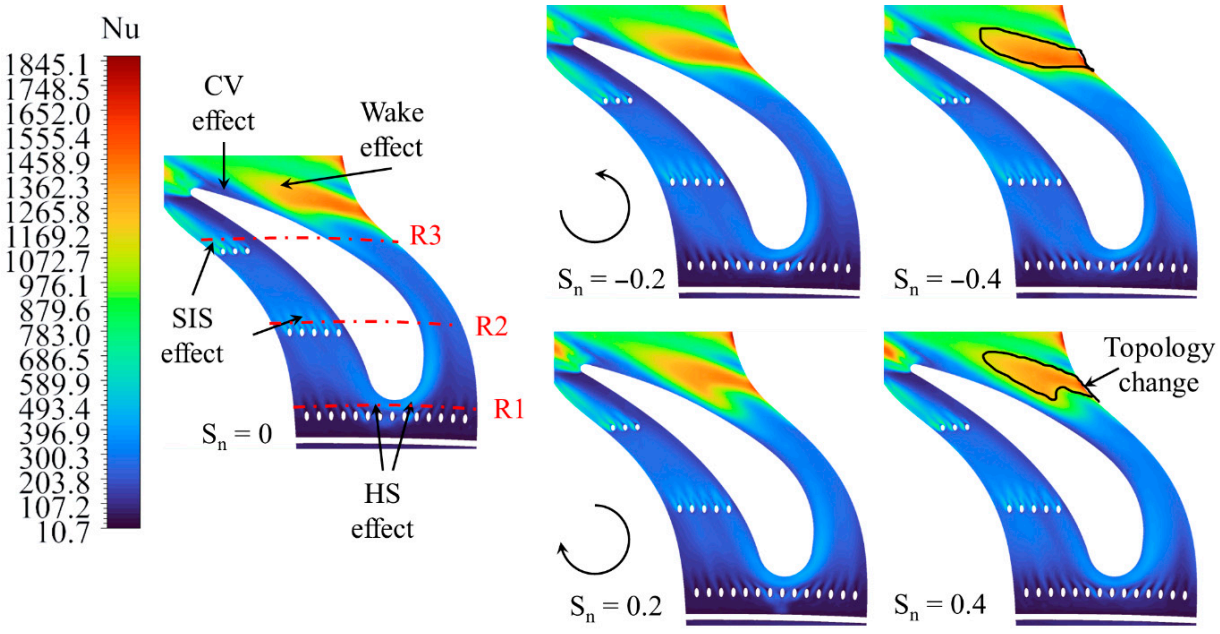

Figure 11. Nusselt number distribution on the hub surface for all the cases.

To quantitatively analyse the local surface heat transfer Nu profiles at three locations downstream of the cooling rows, denoted as R1, R2, and R3 in Figure 11, they are plotted and presented in Figure 12. Downstream of the first cooling row at R1 (Figure 12a), the positive swirl was found to increase the heat transfer at the PS, whereas the negative swirl was found to increase the heat transfer at the SS. Around the LE the swirl effect is negligible. Downstream of the second cooling row at R2 (Figure 12b), the swirl does not have a remarkable effect on the Nu profiles around PS, but it is shown to promote higher heat transfer near the SS when it is clockwise (positive swirl). Close to the TE at R3 (Figure 12c) the results show that the highest surface heat transfer at the SS corner is achieved by the positive swirl with Nu reaching a maximum of 601 and 564 for Sn = 0.4 and 0.2, respectively, whereas Sn = −0.4 and −0.2 only reach maxima of 418 and 360, respectively.

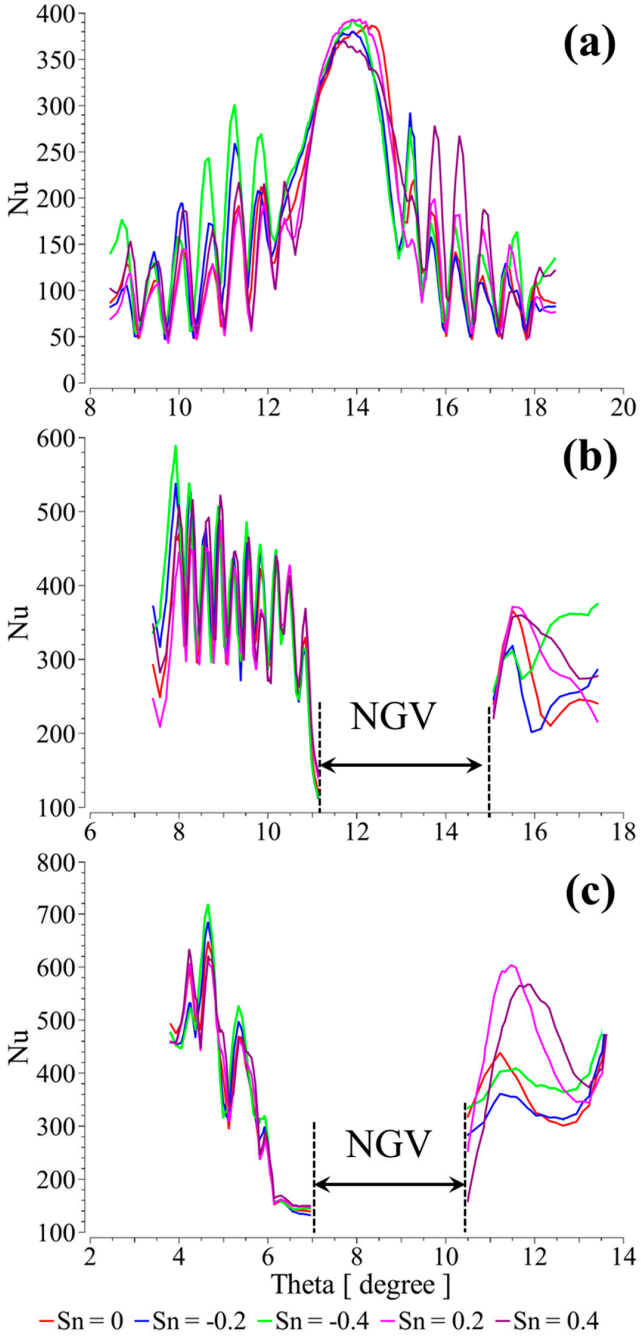

Figure 12. Nusselt number profiles at different locations downstream the cooling rows.

3.6. Effect of the Swirl the Vane Aerodynamic Losses

To further assess the effect of swirl intensity on the aerothermal performance of the film-cooled turbine vane, the aerodynamic loss analysis in crucial. Our previous work [22] provided a more detailed explanation of the loss behaviour in terms of secondary flow structures, which can be summarised herein. The mechanism of aerodynamic loss under varying swirl conditions was primarily associated with the formation of the swirl vortex (SV). The SV originated near the mid-span of the vane leading edge and developed into a double-leg structure, with each leg extending along both the pressure and suction sides of the vane. The direction and intensity of the inlet swirl governed the radial migration of the legs as follows: negative swirl drove the suction-side leg towards the hub, while positive swirl directed it towards the shroud. Overall, the SV generated under negative swirl exhibited higher intensity than that produced under positive swirl, resulting in higher in aerodynamic losses. Indeed, Figure 13 confirms the discussed findings. It reports the total pressure loss coefficient calculated at the cascade exit for all the investigated cases. It can be seen that the axial flow case generates the lowest losses as expected and in line with the findings in the literature. When the swirl is introduced, the aerodynamics losses increase. The negative swirl generates the highest losses, reaching 1.74% and 5.78% higher losses at Sn = −0.2 and −0.4 respectively, relative to the baseline case. The positive swirl exhibits lower losses compared with the negative swirl, reaching 1.14% and 4.42%, higher losses at Sn = 0.2 and 0.4 respectively, relative to the baseline case. Hence, the negative swirl (Sn = −0.4) produces the highest aerodynamic loss, whereas the positive swirl (Sn = 0.2) results in the lowest. This suggests that the combustor nozzle should operate at relatively low swirl numbers to maximise the aerodynamic efficiency of the turbine.

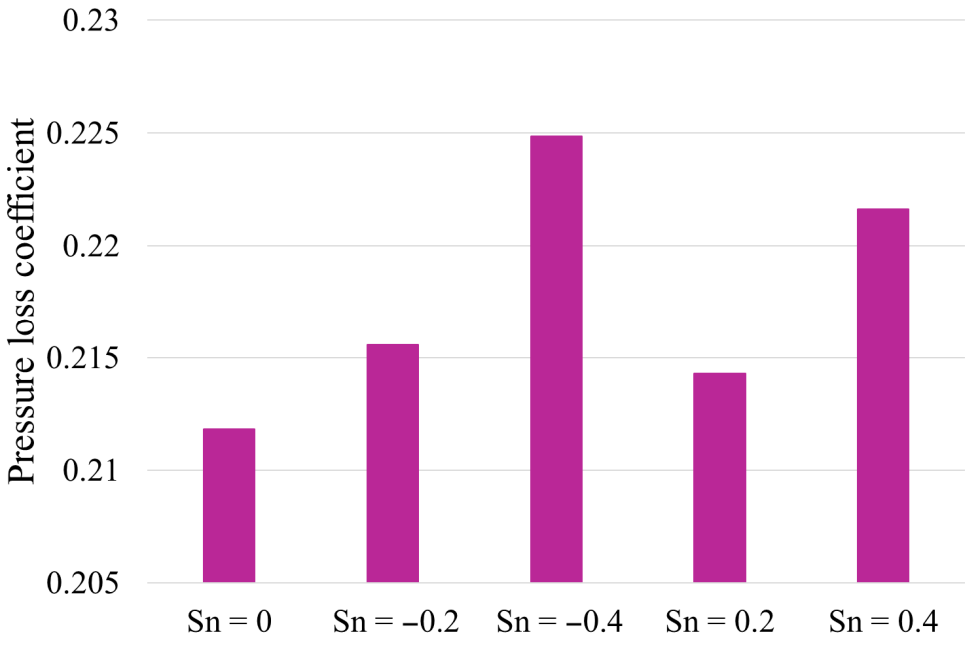

Figure 13. Total pressure loss coefficient at the cascade exit under different axial and swirl conditions.

4. Conclusions

This study employed steady, compressible RANS simulations using ANSYS CFX 19.R3, with the k-ω SST turbulence model coupled with Gamma-Theta transition formulation to capture boundary layer effects. The geometry consisted of a first-stage high-pressure turbine nozzle guide vane with a contoured hub platform and multiple hub film-cooling rows,

designed to replicate modern turbine stages. Swirling inflow conditions of varying intensities and directions were imposed to investigate their influence on aerothermal performance.

The presence of swirl was found to strongly influence local and area-averaged film cooling effectiveness (FCE). Axial flow provided the highest overall FCE, while negative swirl improved cooling at the suction-side corner but reduced effectiveness on the PS. Conversely, positive swirl enhanced pressure-side FCE while diminishing suction-side protection. These results demonstrate a clear directional trade-off in local thermal management associated with the swirl characteristics.

Analysis of the vane–hub corner revealed that swirl direction strongly modulates thermal loading through its influence on boundary layer dynamics. Negative swirl promoted the dominance of the cooler hub boundary layer within the corner vortex, reducing thermal stress at the suction-side corner. Positive swirl, in contrast, energised the suction-side boundary layer, increasing local thermal loading, consistent with observed corner cracks in out-of-service NGVs. While swirl did not suppress the formation of the corner vortex, it modified its thermal topology, altering the interaction between hot and cool boundary layers and thereby governing the local heat transfer.

Swirling inflow increased total pressure losses relative to the axial baseline. Negative swirl generated the highest aerodynamic losses due to an intensified swirl vortex, whereas positive swirl induced moderately higher losses. These findings indicate that improvements in local cooling effectiveness can come at the expense of overall aerodynamic efficiency.

Overall, the study emphasises the necessity of balancing thermal protection with aerodynamic penalties. While negative swirl improves cooling at the suction-side corner, it increases losses, whereas positive swirl reduces losses but elevates thermal stress in critical regions. Optimisation of NGV design thus requires careful consideration of both swirl direction and intensity alongside hub-cooling strategies to ensure both durability and efficiency in modern high-pressure turbine stages.

Author Contributions: D.M., Data Curation, Formal Analysis, Investigation, Visualisation and Writing—Original Draft; Z.M., Conceptualisation, Methodology, Investigation, Resources, Software, Supervision, Validation, Writing—Original Draft, Writing—Review and Editing; S.A., Funding Acquisition, Project Administration, Supervision, Writing—Review and Editing. All authors have read and agreed to the published version of the manuscript.

Funding: This research was funded by the Algerian Ministry of Higher Education and Scientific Research.

Data Availability Statement: Data are available upon request from the authors.

Acknowledgments: The authors would like to extend their gratitude to the higher education and research bodies who supported this research: Algerian Ministry of Higher Education and Scientific Research and Nottingham Trent University (UK).

Conflicts of Interest: The authors declare no conflicts of interest.

Abbreviations

BL	Boundary layer
BR	Blowing ratios
CFD	Computational fluid dynamics
CV	Corner vortex
FCE	Film-cooling effectiveness
HP	High pressure
HPT	High-pressure turbine
HTC	Heat transfer coefficient
LE	Leading edge

MFR	Mass flow ratios
NGV	Nozzle guide vane
NOx	Nitrogen oxides
OTRF	Oxford Turbine Research Facility
PR	Pressure ratio
PS	Pressure side
RANS	Reynolds-Averaged Navier–Stokes
RMS	Root mean square.
SIS	Super-imposed stream
SS	Suction side
SV	Swirl vortex
TE	Trailing edge
TKE	Turbulent kinetic energy
Symbols	
C_{ax}	Vane axial chord (m)
N_u	Nusselt number
S_n	Swirl number
T_∞	Hot mainstream (K)
T_c	Coolant temperatures (K)
u_∞	Mainstream velocity (m/s)
u_c	Coolant velocity (m/s)
HTC	Heat transfer coefficient ($W \cdot m^{-2} \cdot K^{-1}$)
Q	Heat flux ($W \cdot m^{-2}$)
T_{wall}	Cooled hub (surface) temperature (K)
T_{flow}	Near-wall flow temperature (K)
U	Averaged axial velocity (m/s)
W	Averaged tangential velocity (m/s)
v^*	Characteristic velocity in the logarithmic layer of the boundary layer
y^+	Dimensionless height of the first cell
ΔT	Temperature differential between the fluid and the NGV wall (K)
Greek Symbols	
ρ_∞	Mainstream density ($kg \cdot m^{-3}$)
ρ_c	Coolant density ($kg \cdot m^{-3}$)
c_p	Specific heat capacity of the fluid ($J \cdot kg^{-1} \cdot K^{-1}$)
η	Film-cooling effectiveness
λ	Thermal conductivity of the hot fluid ($W \cdot m^{-1} \cdot K^{-1}$)
Subscripts	
c	Coolant
∞	Mainstream (freestream)

References

1. Lazik, W.; Doerr, T.; Bake, S.; Bank, R.V.D.; Rackwitz, L. Development of Lean-Burn Low-NOx Combustion Technology at Rolls-Royce Deutschland. In *ASME Turbo Expo 2008: Power for Land, Sea, and Air*; American Society of Mechanical Engineers Digital Collection: Berlin, Germany, 2009; pp. 797–807. [CrossRef]
2. Khanal, B.; He, L.; Northall, J.; Adami, P. Analysis of Radial Migration of Hot-Streak in Swirling Flow Through High-Pressure Turbine Stage. *J. Turbomach.* **2013**, *135*, 041005. [CrossRef]
3. Zhang, S.; Ding, S.; Liu, P.; Qiu, T. Effects of swirl and hot streak on thermal performances of a high-pressure turbine. *Chin. J. Aeronaut.* **2023**, *36*, 250–267. [CrossRef]
4. Qureshi, I.; Smith, A.D.; Povey, T. HP Vane Aerodynamics and Heat Transfer in the Presence of Aggressive Inlet Swirl. *J. Turbomach.* **2012**, *135*, 021040. [CrossRef]
5. Qureshi, I.; Beretta, A.; Chana, K.; Povey, T. Effect of Aggressive Inlet Swirl on Heat Transfer and Aerodynamics in an Unshrouded Transonic HP Turbine. *J. Turbomach.* **2012**, *134*, 061023. [CrossRef]
6. Beard, P.F.; Smith, A.D.; Povey, T. Effect of Combustor Swirl on Transonic High Pressure Turbine Efficiency. *J. Turbomach.* **2013**, *136*, 011002. [CrossRef]

7. Schmid, G.; Schiffer, H.-P. Numerical Investigation of Inlet Swirl in a Turbine Cascade. In *ASME Turbo Expo 2012: Turbine Technical Conference and Exposition*; American Society of Mechanical Engineers Digital Collection: Copenhagen, Denmark, 2013; pp. 543–552. [CrossRef]
8. Jacobi, S.; Mazzoni, C.; Rosic, B.; Chana, K. Investigation of Unsteady Flow Phenomena in First Vane Caused by Combustor Flow with Swirl. *J. Turbomach.* **2017**, *139*, 041006. [CrossRef]
9. Ito, S.; Goldstein, R.J.; Eckert, E.R.G. Film cooling of a gas turbine blade. *J. Eng. Gas Turbines Power* **1978**, *100*, 476–481. [CrossRef]
10. Hou, R.; Wen, F.; Luo, Y.; Wang, S. Influence of Inlet Swirl on Film Cooling of the Turbine Leading Edge. *Heat Transf. Eng.* **2021**, *42*, 985–1001. [CrossRef]
11. Bacci, T.; Becchi, R.; Picchi, A.; Facchini, B. Adiabatic Effectiveness on High-Pressure Turbine Nozzle Guide Vanes under Realistic Swirling Conditions. *J. Turbomach.* **2019**, *141*, 011009. [CrossRef]
12. Du, K.; Zhang, R.; Jia, Y.; Liu, C.; Sunden, B. Effect of non-axisymmetric endwall contouring and swirling inlet flow on film cooling performance of turbine endwall. *Int. J. Heat Mass Transf.* **2024**, *229*, 125702. [CrossRef]
13. Xu, Z.; Liu, C.; Ye, L.; Zhu, H.; Wu, Z. Investigation of the effect of combustor swirl flow on turbine vane full coverage film cooling. *Energy* **2024**, *295*, 130965. [CrossRef]
14. Lu, X.; Jia, Y.; Ji, Y.; Ge, B.; Zang, S. Effect of the hole configurations on effusion cooling effectiveness under swirl impact in gas turbine combustor. *Int. J. Therm. Sci.* **2024**, *203*, 109164. [CrossRef]
15. Insinna, M.; Griffini, D.; Salvadori, S.; Martelli, F. On the Effect of an Aggressive Inlet Swirl Profile on the Aero-thermal Performance of a Cooled Vane. *Energy Procedia* **2015**, *81*, 1113–1120. [CrossRef]
16. Giller, L.; Schiffer, H.-P. Interactions Between the Combustor Swirl and the High Pressure Stator of a Turbine. In *ASME Turbo Expo 2012: Turbine Technical Conference and Exposition*; American Society of Mechanical Engineers Digital Collection: Copenhagen, Denmark, 2013; pp. 1401–1415. [CrossRef]
17. Li, Z.; Zhang, K.; Li, Z.; Li, J.; Song, L. Effects of Anticlockwise Swirling Inflow on the Aerothermal Performance of the Turbine Vane Endwall with Film Cooling Layouts. In Proceedings of the GPPS Xi'an21, Xi'an, China, 18–20 October 2022. [CrossRef]
18. Werschnik, H.; Hilgert, J.; Wilhelm, M.; Bruschewski, M.; Schiffer, H.-P. Influence of Combustor Swirl on Endwall Heat Transfer and Film Cooling Effectiveness at the Large Scale Turbine Rig. *J. Turbomach.* **2017**, *139*, 081007. [CrossRef]
19. Werschnik, H.; Hilgert, J.; Bruschewski, M.; Schiffer, H.-P. Combustor-Turbine Aerothermal Interaction in an Axial Turbine: Influence of Varied Inflow Conditions on Endwall Heat Transfer and Film Cooling Effectiveness. In *ASME Turbo Expo 2016: Turbomachinery Technical Conference and Exposition*; American Society of Mechanical Engineers Digital Collection: Seoul, Republic of Korea, 2016. [CrossRef]
20. Werschnik, H.; Schiffer, H.-P.; Steinhausen, C. Robustness of a Turbine Endwall Film Cooling Design to Swirling Combustor Inflow. *J. Propuls. Power* **2017**, *33*, 917–926. [CrossRef]
21. Zhang, Y.; Li, Y.; Bian, X.; Yuan, X. Effects of Inlet Swirl on Endwall Film Cooling in Neighboring Vane Passages. In *ASME Turbo Expo 2017: Turbomachinery Technical Conference and Exposition*; American Society of Mechanical Engineers Digital Collection: Charlotte, NC, USA, 2017. [CrossRef]
22. Mansouri, Z.; Belamadi, R. The influence of inlet swirl intensity and hot-streak on aerodynamics and thermal characteristics of a high pressure turbine vane. *Chin. J. Aeronaut.* **2021**, *34*, 66–78. [CrossRef]
23. Mansouri, Z. Numerical prediction of heat transfer characteristics on a turbine nozzle guide vane under various combustor exit hot-streaks. *Heat Transf.* **2022**, *51*, 976–997. [CrossRef]
24. Mansouri, Z.; Jefferson-Loveday, R. Heat transfer characteristics of a high-pressure turbine under combined distorted hot-streak and residual swirl: An unsteady computational study. *Int. J. Heat Mass Transf.* **2022**, *195*, 123143. [CrossRef]
25. Mansouri, Z. Unsteady simulation of flow and heat transfer in a transonic turbine stage under non-uniform inlet conditions. *Int. Commun. Heat Mass Transf.* **2021**, *129*, 105660. [CrossRef]
26. Goldman, L.J.; Mclallin, K.L. *Cold Air Annular Cascade Investigations of Aerodynamic Performance of Core-Engine-Cooled Turbine Vanes*; No NASA TM X-3224; NASA Lewis Research Center: Washington, DC, USA, 1975.
27. Goldman, L.J.; Seasholtz, R.G. *Laser Anemometer Measurements in an Annular Cascade of Core Turbine Vanes and Comparison with Theory*; No NASA-TP-2018; NASA Lewis Research Center: Washington, DC, USA, 1982.
28. Mansouri, Z.; Aouissi, M.; Boushaki, T. A Numerical Study of Swirl Effects on the Flow and Flame Dynamics in a Lean Premixed Combustor. *Int. J. Heat Technol.* **2016**, *34*, 227–235. [CrossRef]
29. Mansouri, Z.; Aouissi, M.; Boushaki, T. Numerical computations of premixed propane flame in a swirl-stabilized burner: Effects of hydrogen enrichment, swirl number and equivalence ratio on flame characteristics. *Int. J. Hydrogen Energy* **2016**, *41*, 9664–9678. [CrossRef]
30. Mansouri, Z.; Boushaki, T. Experimental and numerical investigation of turbulent isothermal and reacting flows in a non-premixed swirl burner. *Int. J. Heat Fluid Flow* **2018**, *72*, 200–213. [CrossRef]
31. Menter, F.R.; Langtry, R.B.; Likki, S.R.; Suzen, Y.B.; Huang, P.G.; Völker, S. A Correlation-Based Transition Model Using Local Variables—Part I: Model Formulation. *J. Turbomach.* **2004**, *128*, 413–422. [CrossRef]

32. Langtry, R.B.; Menter, F.R. Correlation-Based Transition Modeling for Unstructured Parallelized Computational Fluid Dynamics Codes. *AIAA J.* **2009**, *47*, 2894–2906. [CrossRef]
33. Du, K.; Pei, X.; Li, Y.; Liu, C.; Sunden, B. Endwall film cooling performance considering the effects of micro-riblets configurations and layouts. *Int. J. Heat Fluid Flow* **2024**, *108*, 109440. [CrossRef]
34. Zhou, W.; Qenawy, M.; Shao, H.; Peng, D.; Wen, X.; Liu, Y. Turbine vane endwall film cooling with barchan-dune shaped ramp in a single-passage transonic wind tunnel. *Int. J. Heat Mass Transf.* **2020**, *162*, 120350. [CrossRef]
35. Du, K.; Jia, Y.; Liu, C.; Sunden, B. Non-axisymmetric Endwall film cooling characteristics considering the influences of cylindrical holes and laidback fan-shaped holes. *Int. J. Heat Mass Transf.* **2024**, *225*, 125403. [CrossRef]
36. Du, K.; Li, J. Numerical study on the effects of slot injection configuration and endwall alignment mode on the film cooling performance of vane endwall. *Int. J. Heat Mass Transf.* **2016**, *98*, 768–777. [CrossRef]
37. Feng, M.; Dai, X.; Zhang, F.; Liao, G.; E, J. Numerical investigation on film cooling and aerodynamic performance for gas turbine endwalls with upstream vane-type and cascade-type slots. *Aerosp. Sci. Technol.* **2024**, *145*, 108857. [CrossRef]
38. Arrif, K.-E.; Mansouri, Z.; Azzouz, S. Numerical Investigations of the Aerothermal Performance of Modern Turbine Blade Tip Geometries at Design and Off-Design Conditions and Under Stationary and Moving Shroud. *Heat Transf.* **2025**, *54*, 3193–3207. [CrossRef]